PHYSICAL REVIEW B **94**, 020503(R) (2016)

Pressure-induced superconductivity in the antiferromagnet κ-$(ET)_2CF_3SO_3$ with quasi-one-dimensional triangular spin lattice

Hiroshi Ito,[1] Takayuki Asai,[1] Yasuhiro Shimizu,[2] Hiromi Hayama,[3] Yukihiro Yoshida,[3] and Gunzi Saito[3,4]

[1]*Department of Applied Physics, Nagoya University, Furo-cho, Chikusa-ku, Nagoya 464-8603, Japan*

[2]*Department of Physics, Graduate School of Science, Nagoya University, Furo-cho, Chikusa-ku, Nagoya 464-8602, Japan*

[3]*Faculty of Agriculture, Meijo University, Shiogamaguchi 1-501 Tempaku-ku, Nagoya 468-8502, Japan*

[4]*Toyota Physical and Chemical Research Institute, 41-1, Yokomichi, Nagakute, Aichi 480-1192, Japan*

(Received 30 July 2015; revised manuscript received 22 June 2016; published 18 July 2016)

We report an antiferromagnetic (AF) ordering at ambient pressure and a superconducting transition under pressure for κ-$(ET)_2CF_3SO_3$ [ET = bis(ethylenedithio)tetrathiafulvalene], which has a two-dimensional electronic system with quasi-one-dimensional triangular spin lattice. At ambient pressure, AF ordering was detected at $T_N = 2.5$ K by ^{1}H NMR, subsequent to two structural phase transitions at 230 and 190 K. Under hydrostatic pressures, metallic behavior appeared above ~1.1 GPa, and a superconducting transition (maximum onset $T_c = 4.8$ K at ~1.3 GPa) was observed up to 2.2 GPa. Superconductivity was also found under c-axis strain, which reduced t'/t, but was absent under b-axis strain which increased t'/t.

DOI: 10.1103/PhysRevB.94.020503

κ-type bis(ethylenedithio)tetrathiafulvalene (ET) salts have a two-dimensional (2D) electronic system showing unconventional superconductivity (SC) near the Mott insulator region, with an on-site Coulomb energy U comparable to the upper bandwidth W [1–3]. In κ-$(ET)_2X$ (X = monoanion), ET dimers have a spin unit ($S = 1/2$) and form a triangular spin lattice with interdimer transfer integrals t and t', as shown in Fig. 1(a) [2]. When the triangle is equilateral with $t'/t \approx 1$, the geometric spin frustration prevents long-range antiferromagnetic (AF) ordering, and a quantum spin liquid (QSL) phase may appear [4]. QSL behavior was first observed in κ-$(ET)_2Cu_2(CN)_3$ [5]. Since then, QSL candidates have been reported among both organic and inorganic materials, such as $EtMe_3Sb[Pd(dmit)_2]_2$ (dmit = 1,3-dithiole-2-thione-4,5-dithiolate) [6], κ-$H_3(Cat\text{-}EDT\text{-}TTF)_2$ (H_2Cat-EDT-TTF = catechol-fused ethylenedithiotetrathiafulvalene) [7], $ZnCu_3(OH)_6Cl_2$ [8], and $Na_4Ir_3O_8$ [9]. In addition, many theoretical studies have been carried out to establish the phase diagram as a function of t'/t and U/W (or U/t) [10–13].

The Heisenberg magnet Cs_2CuCl_4, which has a quasi-one-dimensional (Q1D) spin lattice characterized with $t'/t = 1.71$, has also attracted attention [14]. In Heisenberg magnets having an infinitely large U/t, the anisotropic spin lattice will release the spin frustration and induce AF ordering, as is observed in Cs_2CuCl_4 ($T_N = 0.62$ K). On the other hand, large t'/t is expected to enhance the Q1D spin fluctuation, which could inhibit long-range AF ordering. Cs_2CuCl_4 has prompted theoretical interests in Q1D triangular spin lattices in the $t'/t > 1$ range [15–17].

Recently, we obtained κ-$(ET)_2B(CN)_4$, which forms a Q1D triangular spin lattice ($t'/t = 1.42$ at room temperature) exhibiting a valence bond crystal ground state below 5 K [18]. In the present Rapid Communication, we focus on κ-$(ET)_2CF_3SO_3$, on which there has been no follow-up since the first report in 1995 [19]. The triangular spin lattice of κ-$(ET)_2CF_3SO_3$ has the highest t'/t among κ-$(ET)_2X$, i.e., 1.79 (extended Hückel calculation [20] at 298 K), which is close to that for Cs_2CuCl_4, but κ-$(ET)_2CF_3SO_3$ has a moderate $U/W = 0.852$ ($U/t = 9.96$). At ambient pressure, ^{1}H NMR detected AF ordering at $T_N = 2.5$ K, in contrast to κ-$(ET)_2B(CN)_4$. The electrical transport was 2D-like, exhibiting metallic behavior under hydrostatic pressures above ~1.1 GPa and an SC transition was observed at $T_c = 4.8$ K (onset at ~1.3 GPa). These results provide insight into the interplay between AF ordering, spin frustration, and SC in κ-$(ET)_2X$ in an unexplored area of the triangular spin lattice phase diagram, i.e., at $t'/t > 1$.

Rhombic plate-shaped single crystals were obtained as a minor product by electrooxidation of ET with the electrolyte $(Bu_4N)CF_3SO_3$ in 1,1,2-trichloroethane [19]. The major product, needlelike crystals of δ-$(ET)_2CF_3SO_3$ [21], was separated under a microscope. X-ray diffraction experiments were performed on a CCD-type diffractometer (Bruker SMART APEX II) with graphite-monochromated Mo $K\alpha$ radiation ($\lambda = 0.71073$ Å) in the range of 100–298 K cooled with nitrogen gas. The crystal structures were solved by a direct method using the SIR2004 program [22] and were refined by a full-matrix least-squares method on F^2 using the SHELXL program [23]. All nonhydrogen atoms were anisotropically refined. ^{1}H and ^{19}F NMR measurements were performed on a polycrystalline sample under a magnetic field of 2.0 T. The NMR spectra were obtained by Fourier transformation of solid-echo signals. The ^{1}H and ^{19}F nuclear spin-lattice relaxation rates, denoted by $^1T_1^{-1}$ and $^{19}T_1^{-1}$, respectively, were obtained by using the saturation recovery method. Electron paramagnetic resonance (EPR) measurements were performed on a single crystal aligned with respect to the external magnetic field using an X-band spectrometer equipped with a gas flow cryostat. The absolute magnitude of the spin susceptibility was calibrated using $CuSO_4 \cdot 5H_2O$. For the magnetic measurements, the typical sample cooling rate was 10 K min^{-1}. The four-probe resistivity at a dc current of 0.001–0.1 mA was measured using platinum wires attached to a single crystal with graphite paste. The hydrostatic pressure was applied via Daphne 7373 oil using a BeCu clamp cell with a NiCrAl inner core. The pressure was monitored at room temperature and was presumably reduced by about 0.2 GPa at low temperatures. Uniaxial compression was applied using the epoxy (Stycast 1266) encapsulation method [24]. For the

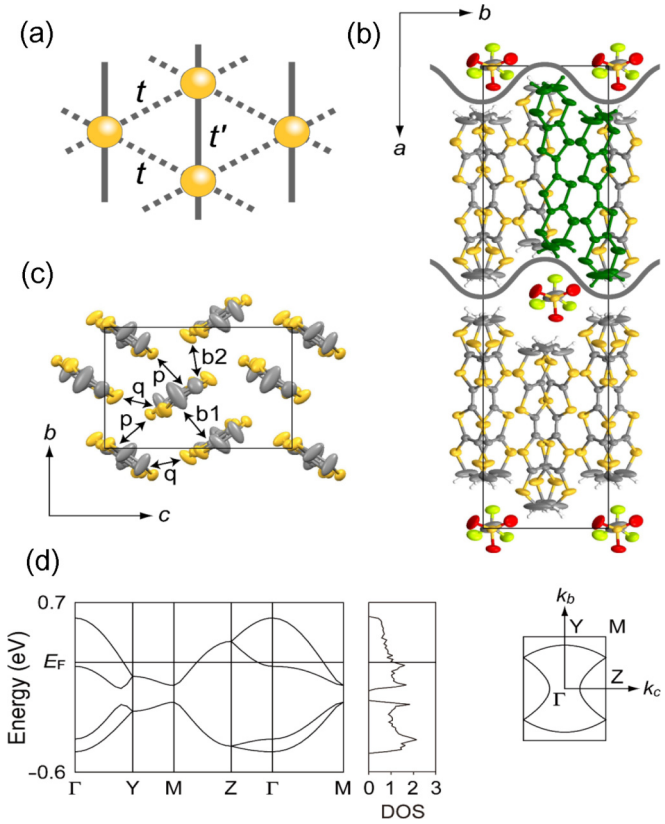

FIG. 1. (a) Schematic of the triangular spin lattice, where circles show the $(ET)_2^{\bullet+}$ dimers. (b) Crystal structure of κ-$(ET)_2CF_3SO_3$ at 298 K, viewed along the c axis, where only one orientation of the disordered CF_3SO_3 anion is shown. Two dark-green ET molecules form a dimer and the gray lines indicate the wavy surface of ET layers. (c) Projected view of ET molecules along the molecular long axis with directions of interactions ($b1$, $b2$, p, and q). Hydrogen atoms are omitted. (d) Energy dispersion, density of states (DOS), and Fermi surface calculated at 298 K. The unit of DOS is states eV^{-1} $spin^{-1}$.

resistivity measurements, the typical temperature sweep rate was 0.5 K min^{-1}.

Figure 1(b) shows the crystal structure of κ-$(ET)_2CF_3SO_3$ at 298 K, viewed along the c axis [25]. 2D layers of ET molecules on the bc plane are separated by discrete CF_3SO_3 anions. In each layer, ET molecules are arranged in a κ-type packing motif of orthogonal $(ET)_2^{\bullet+}$ dimers, as seen in Fig. 1(c). The transfer integrals between ET molecules within the layer calculated by the extended Hückel method [20] are shown in Table I. The t'/t value is 1.79 at 298 K (1.30 by first-principles calculation [26]), where $t = (|t_p| + |t_q|)/2$ and $t' = t_{b2}/2$. We note that discrete anions CF_3SO_3 make corrugated 2D sheets of ET dimers, as in the case of κ-$(ET)_2B(CN)_4$ [18]. As seen in Fig. 1(b), an anion molecule in the upper anion layer pushes down an ET molecule and a corresponding anion molecule in the lower anion layer pushes up the other ET molecule in a dimer. Thus, ET molecules within a dimer (shown in dark-green) deviate toward each other along the molecular long axis of ET, suppressing the intradimer overlap integral, i.e., the U in the dimer model. At the same time, the transfer integral between dimers, t', is enhanced, leading to a Q1D spin lattice. Despite the Q1D nature of the triangular spin lattice, a 2D electronic structure shown in Fig. 1(d) is calculated like other κ-$(ET)_2X$.

At 298 K, it is likely that the anions were disordered by a dynamical rotation around the C-S bond [27]; CF_3 and SO_3 groups are crystallographically indistinguishable. Upon cooling, the anions were frozen into an ordered form at ~230 K, changing the crystal space group from $C2/c$ to $P2_1/c$. The $P2_1/c$ phase comprises two kinds of alternating ET layers with different t'/t. The calculated band structure for each layer retains the 2D nature similar to that at 298 K. Below ~190 K, a further structural transition occurred, inducing sixfold periodicity along the b axis [28]. The $6 \times b$ superstructure exists at least down to 34 K [29].

Figure 2(a) shows ^{19}F NMR spectra above 180 K. The spectra exhibited an abrupt broadening below 210 K, indicating that the rotational motion of the CF_3 group slowed down well below an NMR frequency, ν_0, of 80.4 MHz. This is reflected by the $^{19}T_1^{-1}$ peak around 250 K [Fig. 2(b)]. The motional contribution was suppressed below 150 K, which indicates that the $^1T_1^{-1}$ behavior below the temperature was governed by spin fluctuations. Below 100 K, $^1T_1^{-1}$ was nearly constant down to 10 K, which agrees with the behavior of a 1D QSL [30] or 2D quantum antiferromagnet [31] in the critical regime. With a further decrease in temperature, the ^1H NMR spectrum showed a prominent broadening below 3 K, as shown in Fig. 2(c). $^1T_1^{-1}$ exhibited a sharp peak at 2.5 K, owing to the critical slowdown in spin fluctuations [Fig. 2(b)]. These results provide clear evidence of a long-range AF order below 2.5 K.

Figure 2(d) shows the EPR spin susceptibility (χ) in a magnetic field along the a^* axis. The temperature dependence of χ behaved as the $S = 1/2$ Heisenberg antiferromagnet on a triangular lattice with $|J|/k_B = 200$ K [32], as represented by the solid line in Fig. 2(d). This suggests that the present compound can be regarded as a frustrated Mott insulator with a spin-1/2 on each ET dimer. As reported previously [19], the EPR line broadened below 200 K and the linewidth showed a maximum at ~80 K in the magnetic field along the a^* axis. On the other hand, the linewidth continued to increase at low

TABLE I. Band parameters of κ-$(ET)_2CF_3SO_3$ calculated by the extended Hückel method.

T (K)	Space group	Layer	t_{b1} (eV)	t_{b2} (eV)	t_p (eV)	t_q (eV)	t'/t	U/W	U/t
298	$C2/c$		0.230	0.166	0.034	−0.058	1.79	0.852	9.96
250	$C2/c$		0.239	0.169	0.034	−0.058	1.84	0.877	10.4
200	$P2_1/c$	A	0.234	0.157	0.029	−0.077	1.50	0.842	8.89
		B	0.248	0.169	0.048	−0.047	1.77	0.893	10.4

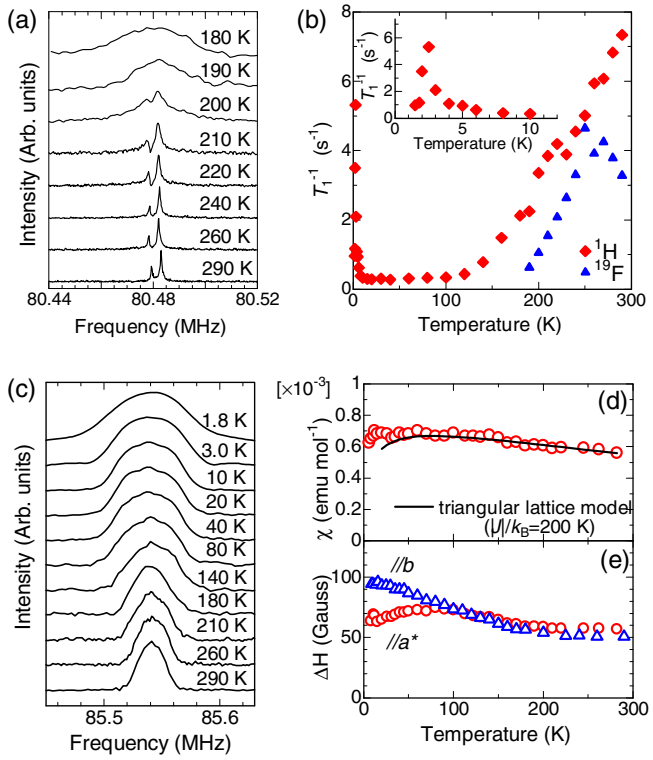

FIG. 2. Temperature dependence of (a) ^{19}F NMR spectra, (b) ^{19}F and ^{1}H nuclear spin-lattice relaxation rates, (c) ^{1}H NMR spectra, (d) EPR spin susceptibility (χ), where the solid line represents the fit to the triangular lattice model [32], and (e) EPR linewidth (ΔH) under magnetic fields along the a^* (circles) and b (triangles) axes.

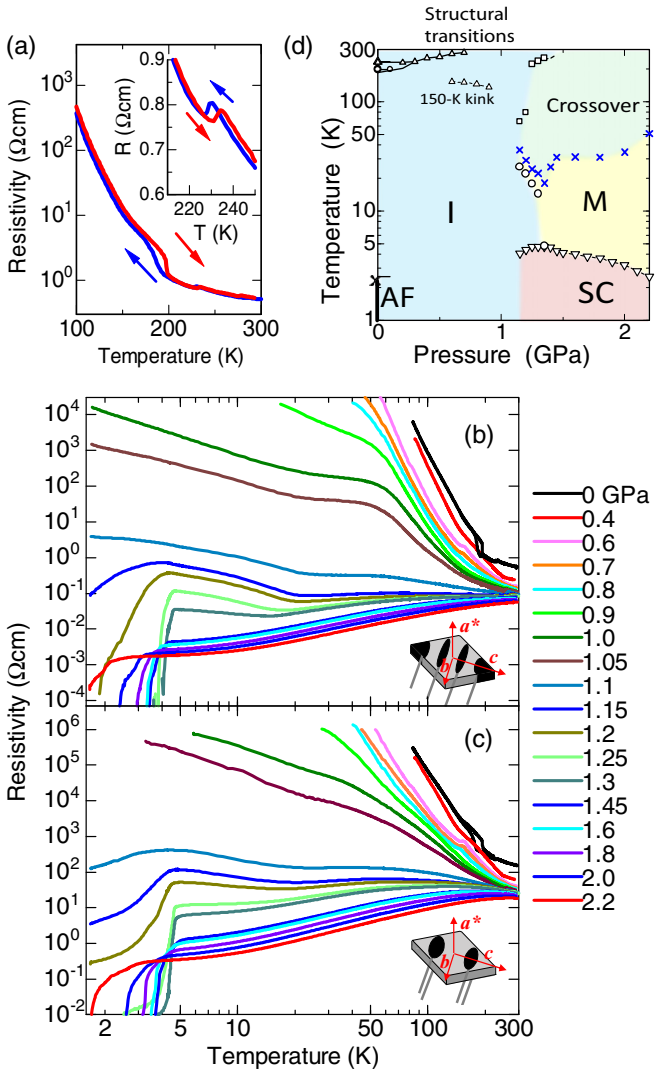

FIG. 3. (a) Temperature dependence of the c-axis resistivity at ambient pressure. The inset is a blowup around the transition at 230 K. Temperature dependence of (b) c-axis and (c) a^*-axis resistivities under various hydrostatic pressures up to 2.2 GPa. (d) A pressure-temperature state diagram comprising AF, insulating (I), metallic (M), and SC phases and a crossover region between I and M phases characterized by a convex temperature dependence of resistivity, based on the c-axis resistivity measurements.

temperatures in the magnetic field along the b axis, as in the case of other κ-(ET)$_2X$ [33,34], which may be indicative of AF fluctuations.

Figure 3(a) shows the temperature dependence of the in-plane c-axis resistivity at ambient pressure. Typical conductivity values at room temperature were 0.01, 4, and 2 S cm^{-1} along the a^*, b, and c axes, respectively; namely, the ratio of in-plane to interlayer conductivities was ∼300. Two resistivity changes with thermal hysteresis were found near 230 and 190 K, which correspond to the structural transitions. At the 230 K transition, the resistivity decreased by ∼5% upon cooling, presumably because random potentials due to the anion disorder were removed. At the 190 K transition, the resistivity doubled upon cooling, as a result of the $6 \times b$ superstructure formation.

Figures 3(b) and 3(c) show the temperature dependence of the resistivity along the c and a^* axes, respectively, under hydrostatic pressures. The geometries of the electrodes are shown as inset figures. The resistivity changes due to the structural transitions merge as a single kink above 0.3 GPa and the kink temperature increases with increasing pressure up to 0.7 GPa [35]. Between 0.6 and 0.9 GPa, there appeared another kink at ∼150 K. The semiconducting temperature dependence was gradually suppressed by applying pressure and metallic behavior was observed above ∼1.1 GPa. At the same time, a sharp drop in resistivity ascribable to an SC transition appeared below 4 K. At ∼1.3 GPa, T_c showed a maximum of 4.8 K. We note that the critical pressures for the insulator-metal transition and the SC transition showed some sample dependencies (error of ±0.1 GPa). The SC persisted over a wide pressure range of up to 2.2 GPa. Up to ∼1.3 GPa, resistivity showed insulating behavior above T_c, as in the case of κ-(ET)$_2$Cu[N(CN)$_2$]Cl [36]. However, the temperature variation of the resistivity is rather smooth, showing no jumps or hysteresis, unlike κ-(ET)$_2$Cu[N(CN)$_2$]Cl [36] and κ-(ET)$_2$Cu$_2$(CN)$_3$ [34,37] in which a first-order insulator-metal transition was observed. These behaviors were common to resistivities along the c and a^* axes (examined with three samples each), although the a^*- vs c-axis resistivity anisotropy showed some temperature dependence [38]. The resistivity along the b axis (one sample) showed almost the same behavior with that along the c axis, indicating the isotropic electrical

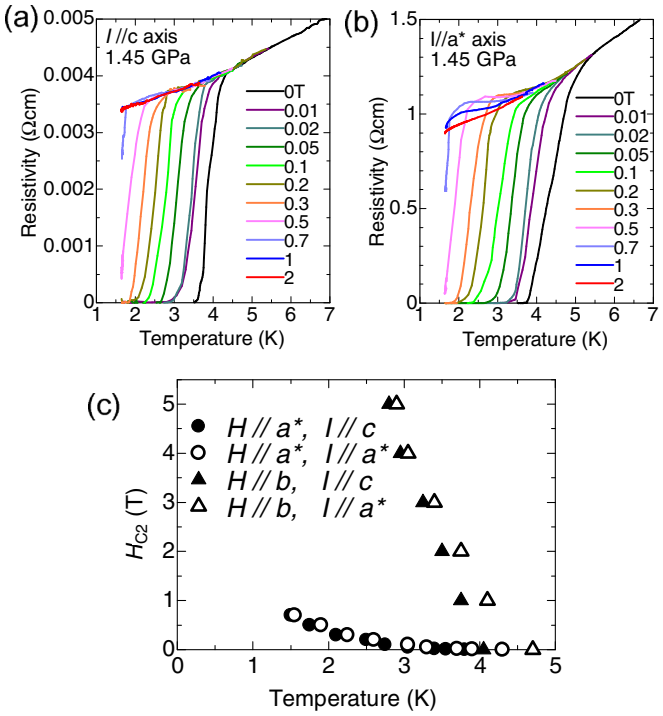

FIG. 4. Temperature dependence of (a) c-axis and (b) a^*-axis resistivities in various magnetic fields applied along the a^* axis. (c) Temperature dependence of upper critical field (H_{c2}) defined as midpoints of the resistive transition for the two current directions in magnetic fields along the a^* and b axes. The crystal axis with respect to the magnetic field was aligned within an error of a few degrees.

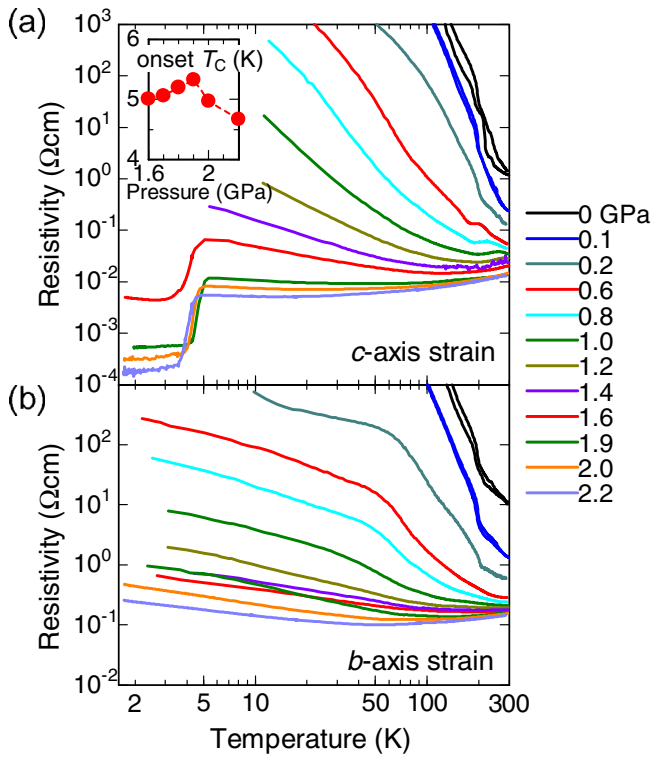

FIG. 5. Temperature dependence of the c-axis resistivity under various uniaxial strains applied along the (a) c axis and (b) b axis. The inset in (a) is the onset T_c versus c-axis strain.

transport within the bc plane under pressure [39]. In Fig. 3(d), we draw a pressure-temperature state diagram based on the c-axis resistivity data.

Figures 4(a) and 4(b) show the resistive SC transition at 1.45 GPa under magnetic fields applied perpendicular to the bc plane, with the current along the c and a^* axes, respectively. We found a resistance hump in the mixed state only when the current was applied along the a^* axis. This is reminiscent of the behavior of κ-$(ET)_2Cu(NCS)_2$ and has been ascribed to the interlayer Josephson coupling [40]. Figure 4(c) plots the magnetic field dependence of T_c, defined as the midpoint of the transition viewed as the temperature dependence of the upper critical field perpendicular ($H_{c2\perp}$) and parallel ($H_{c2\parallel}$) to the bc plane. The slopes of the $H_{c2}(T)$ curves near T_c, in the region of validity of the Ginzburg-Landau theory, allow us to determine the coherence lengths, using the equations [41]

$$-\mu_0 T_c \frac{dH_{c2\perp}}{dT}\bigg|_{T=T_c} = \frac{\phi_0}{2\pi\xi_{\parallel}(0)^2},$$

$$-\mu_0 T_c \frac{dH_{c2\parallel}}{dT}\bigg|_{T=T_c} = \frac{\phi_0}{2\pi\xi_{\parallel}(0)\xi_{\perp}(0)},$$

where $\xi_{\parallel}(0)$ and $\xi_{\perp}(0)$ are the coherence lengths parallel and perpendicular to the layer, respectively, μ_0 is the permeability of vacuum, and ϕ_0 is the magnetic flux quantum; the coherence lengths thus obtained are $\xi_{\parallel}(0) \sim 37 \pm 6$ nm and $\xi_{\perp}(0) \sim 0.7 \pm 0.15$ nm. The interlayer coherence length shorter than the interlayer spacing and a large anisotropy of the inter- and intralayer coherence lengths indicate a 2D nature of SC like other κ-$(ET)_2X$ [41].

Applying uniaxial strain is a powerful technique for studying anisotropic properties. We found a resistivity drop indicative of an SC transition with an onset T_c of 4.8 K under c-axis strains above 1.6 GPa [Fig. 5(a)], which reduces t'/t and thus enhances the triangular spin frustration. T_c exhibits a maximum at 1.9 GPa and the SC persists up to 2.2 GPa. Interestingly, the resistivity drop associated with the SC transition was not observed under a uniaxial strain along the b axis up to 2.2 GPa [Fig. 5(b)], which corresponds to the direction that further increases t'/t.

There are only a few examples of κ-$(ET)_2X$ with $t'/t > 1$, corresponding to a Q1D spin lattice. The other one, κ-$(ET)_2B(CN)_4$, presents a nonmagnetic spin-singlet ground state [18], in contrast to κ-$(ET)_2CF_3SO_3$ in which AF ordering is observed. It is possible that the unconventional AF ordering is realized owing to the bilayer structure; however, the different ground state between the two salts could be ascribed to different temperature dependence of t'/t and U/t in two compounds. Theoretical studies have identified a collinear AF (AFC) phase appearing between nonmagnetic insulator and paramagnetic metal phases for Q1D spin lattice in a parameter region of $1.67 > t'/t > 1.18$ and $U/t \sim 5$ [16] or $t'/t > 1.25$ and $U/t \sim 8$ [17]. At present, the band calculation below 190 K is unavailable due to the $6 \times b$ superstructure; however, it is possible that t'/t and U/t of both layers A and B fall within the range of the AFC state [42]. Thus, the AF ordering in κ-$(ET)_2CF_3SO_3$ can be assigned as the AFC phase.

On the other hand, κ-$(ET)_2B(CN)_4$ does not show an AF ground state presumably because U/t is too large to realize the AFC state at low temperature.

Uniaxial strain results are summarized as follows: κ-$(ET)_2CF_3SO_3$ exhibits SC when t'/t approached unity and no SC when t'/t deviated from unity. This indicates that t'/t approaching unity is favorable for SC. Then, the SC transition under hydrostatic pressure could be understood as a result of the decrease in t'/t at low temperature under hydrostatic pressure: κ-$(ET)_2CF_3SO_3$ could go into the SC area on the theoretically predicted phase diagram [11–13]. On the other hand, κ-$(ET)_2B(CN)_4$ shows no metallic behavior at least up to 2.5 GPa, probably because of large t'/t and U/t at low temperature [18,42].

Evolution of the bilayer structure under pressure is an intriguing issue, especially whether the bilayer structure is present when SC appears. X-ray diffraction study under pressure will undoubtedly be considered in future works. Even if the bilayer structure is present under pressure, it is hard to consider the situation in which only one of the layers shows SC while the other remains insulating, because the behavior of interlayer resistivity is basically similar to that of in-plane resistivity in the whole pressure range as shown in Figs. 3(b) and 3(c). It is possible that bilayered salts possessing alternate metallic and insulating layers show the metallic in-plane and insulating interlayer resistivities [43]. Another possibility, i.e., one is SC while the other is a normal metal, is left, because the anisotropy of the superconducting coherence length is as large as that found for a bilayered $(TMET\text{-}STF)_2BF_4$, in which such electronic state is suggested by the band calculations [44].

In summary, we found an AF ordering at ambient pressure and an SC phase under pressure in κ-$(ET)_2CF_3SO_3$, which shows 2D electrical transport but has a Q1D triangular spin lattice. At ambient pressure, AF ordering was detected at $T_N = 2.5$ K by ^{1}H NMR, subsequent to two structural phase transitions at 230 and 190 K associated with the dynamic disorder of CF_3SO_3 anions. NMR and EPR measurements suggest that the present compound is a frustrated Mott insulator with a spin-1/2 on each ET dimer. At hydrostatic pressures above ~1.1 GPa, the insulating behavior was suppressed, and an SC transition appeared at $T_c = 4.8$ K (onset at ~1.3 GPa). SC was also observed under the c-axis strain, whereas no SC was observed under the b-axis strain. These observations shed light on the interplay between AF ordering, spin frustration, and SC, in an unexplored area of the triangular spin-lattice phase diagram at $t'/t > 1$.

The authors thank K. Sato, H. Tanaka, and S. Kuroda for the EPR measurements. This work was supported by JSPS KAKENHI Grant No. JP23225005, as part of their "Development of Electronic Multifunction Based on Organic Triangular Spin Lattice" program.

[1] T. Ishiguro, K. Yamaji, and G. Saito, *Organic Superconductors*, 2nd ed. (Springer-Verlag, Berlin, 1998).
[2] K. Kanoda and R. Kato, Annu. Rev. Condens. Matter **2**, 167 (2011).
[3] G. Saito and Y. Yoshida, Chem. Rec. **11**, 124 (2011).
[4] P. W. Anderson, Mater. Res. Bull. **8**, 153 (1973).
[5] Y. Shimizu, K. Miyagawa, K. Kanoda, M. Maesato, and G. Saito, Phys. Rev. Lett. **91**, 107001 (2003).
[6] T. Itou, A. Oyamada, S. Maegawa, M. Tamura, and R. Kato, J. Phys.: Condens. Matter **19**, 145247 (2007).
[7] T. Isono, H. Kamo, A. Ueda, K. Takahashi, M. Kimata, H. Tajima, S. Tsuchiya, T. Terashima, S. Uji, and H. Mori, Phys. Rev. Lett. **112**, 177201 (2014).
[8] P. Mandels and F. Bert, J. Phys. Soc. Jpn. **79**, 011001 (2010).
[9] Y. Okamoto, M. Nohara, H. Aruga-Katori, and H. Takagi, Phys. Rev. Lett. **99**, 137207 (2007).
[10] H. Morita, S. Watanabe, and M. Imada, J. Phys. Soc. Jpn. **71**, 2109 (2002).
[11] T. Watanabe, H. Yokoyama, Y. Tanaka, and J. Inoue, J. Phys. Soc. Jpn. **75**, 074707 (2006).
[12] B. Kyung and A.-M. S. Tremblay, Phys. Rev. Lett. **97**, 046402 (2006).
[13] B. J. Powell and R. H. McKenzie, Rep. Prog. Phys. **74**, 056501 (2011).
[14] R. Coldea, D. A. Tennant, A. M. Tsvelik, and Z. Tylczynski, Phys. Rev. Lett. **86**, 1335 (2001).
[15] Y. Hayashi and M. Ogata, J. Phys. Soc. Jpn. **76**, 053705 (2007); D. Heidarian, S. Sorella, and F. Becca, Phys. Rev. B **80**, 012404 (2009).
[16] A. Yamada, Phys. Rev. B **89**, 195108 (2014); **90**, 235138 (2014).
[17] L. F. Tocchio, C. Gros, R. Valenti, and F. Becca, Phys. Rev. B **89**, 235107 (2014).
[18] Y. Yoshida, H. Ito, M. Maesato, Y. Shimizu, H. Hayama, T. Hiramatsu, Y. Nakamura, H. Kishida, T. Koretsune, C. Hotta, and G. Saito, Nat. Phys. **11**, 679 (2015).
[19] M. Fettouhi, L. Ouahab, C. Gómez-García, L. Ducasse, and P. Delhaès, Synth. Met. **70**, 1131 (1995).
[20] T. Mori, A. Kobayashi, Y. Sasaki, H. Kobayashi, G. Saito, and H. Inokuchi, Bull. Chem. Soc. Jpn. **57**, 627 (1984).
[21] D. Chasseau, D. Watkin, M. J. Rosseinsky, M. Kurmoo, D. R. Talham, and P. Day, Synth. Met. **24**, 117 (1988).
[22] M. C. Burla, R. Caliandro, M. Camalli, B. Carrozzini, G. L. Cascarano, L. De Caro, C. Giacovazzo, G. Polidori, and R. Spagna, J. Appl. Crystallogr. **38**, 381 (2005).
[23] G. M. Sheldrick, *SHELXL-2013* (University of Göttingen, Germany, 2013).
[24] M. Maesato, Y. Kaga, R. Kondo, and S. Kagoshima, Rev. Sci. Instrum. **71**, 176 (2000).
[25] Crystal data for κ-$(ET)_2CF_3SO_3$: $C_{21}H_{16}F_3O_3S_{17}$, $M = 918.47$. At 298 K: monoclinic, $C2/c$ (#15), $a = 34.248(3)$ Å, $b = 8.2630(6)$ Å, $c = 11.6857(9)$ Å, $\beta = 99.756(1)^\circ$, $V = 3259.1(4)$ Å^3, $Z = 4$, μ(Mo Kα) = 1.172 mm^{-1}, $R_1 = 0.0451$ [for $I > 2\sigma(I)$], $wR_2 = 0.1204$ (for all data), goodness of fit = 1.043. At 200 K: monoclinic, $P2_1/c$ (#14), $a = 34.130(3)$ Å, $b = 8.1982(6)$ Å, $c = 11.5964(9)$ Å, $\beta = 99.624(1)^\circ$, $V = 3199.1(4)$ Å^3, $Z = 4$, μ(Mo Kα) = 1.194 mm^{-1}, $R_1 = 0.0613$ [for $I > 2\sigma(I)$], $wR_2 = 0.1422$ (for all data), goodness of fit = 1.035.

[26] T. Koretsune and C. Hotta (private communication).
[27] C. I. Ratcliffe and B. A. Dunell, J. Chem. Soc., Faraday Trans. **77**, 2169 (1981).
[28] See Supplemental Material at http://link.aps.org/supplemental/10.1103/PhysRevB.94.020503 for the evolution of the superstructure below 190 K.
[29] M. Watanabe (private communication).
[30] S. Sachdev, Phys. Rev. B **50**, 13006 (1994).
[31] S. Chakravarty, B. I. Halperin, and D. R. Nelson, Phys. Rev. B **39**, 2344 (1989).
[32] N. Elstner, R. R. P. Singh, and A. P. Young, Phys. Rev. Lett. **71**, 1629 (1993).
[33] T. Nakamura, T. Nobutoki, T. Takahashi, G. Saito, H. Mori, and T. Mori, J. Phys. Soc. Jpn. **63**, 4110 (1994).
[34] T. Komatsu, N. Matsukawa, T. Inoue, and G. Saito, J. Phys. Soc. Jpn. **65**, 1340 (1996).
[35] See Supplemental Material at http://link.aps.org/supplemental/10.1103/PhysRevB.94.020503 for the temperature dependence of the c-axis resistivity at low pressure region.
[36] H. Ito, T. Ishiguro, M. Kubota, and G. Saito, J. Phys. Soc. Jpn. **65**, 2987 (1996); F. Kagawa, T. Itou, K. Miyagawa, and K. Kanoda, Phys. Rev. B **69**, 064511 (2004).
[37] Y. Kurosaki, Y. Shimizu, K. Miyagawa, K. Kanoda, and G. Saito, Phys. Rev. Lett. **95**, 177001 (2005).
[38] See Supplemental Material at http://link.aps.org/supplemental/10.1103/PhysRevB.94.020503 for the a^*- vs c-axis resistivity anisotropy.
[39] See Supplemental Material at http://link.aps.org/supplemental/10.1103/PhysRevB.94.020503 for the b-axis resistivity under pressure up to 2.0 GPa.
[40] H. Ito, T. Ishiguro, T. Komatsu, G. Saito, and H. Anzai, Physica B **201**, 470 (1994); S. Friemel, C. Pasquier, and D. Jérome, Physica C **292**, 273 (1997).
[41] K. Oshima, H. Urayama, H. Yamochi, and G. Saito, J. Phys. Soc. Jpn. **57**, 730 (1988); Y. Shimojo, T. Ishiguro, H. Yamochi, and G. Saito, *ibid.* **71**, 1716 (2002).
[42] See Supplemental Material at http://link.aps.org/supplemental/10.1103/PhysRevB.94.020503 for the temperature dependence of t'/t and U/t for various κ-$(ET)_2X$.
[43] R. Lyubovskaya, E. Zhilyaeva, G. Shilov, A. Audouard, D. Vignolles, E. Canadell, S. Pesotskii, and R. Lyubovskii, Eur. J. Inorg. Chem. **2014**, 3820 (2014), and references therein.
[44] S. Uji, C. Terakura, T. Terashima, Y. Okano, and R. Kato, Phys. Rev. B **64**, 214517 (2001).